Jens Bange, Rainer Roth

Helicopter-Borne Flux Measurements in the Nocturnal Boundary Layer over Land - A Case Study

Zuerst erschienen in:
Boundary Layer Meteorology. - Dordrecht : Springer. - Bd. 92 (1999), Nr. 2, S. 295-326
The original publication is available at www.springerlink.com.
DOI: 10.1023/A:1002078712313
http://www.springerlink.com/content/t62v06704p178338/fulltext.pdf

Helicopter-Borne Flux Measurements in the Nocturnal Boundary Layer Over Land - a Case Study

Jens Bange (bange@muk.uni-hannover.de) and Rainer Roth
Institut für Meteorologie und Klimatologie der Universität Hannover, Hannover, Germany

Abstract. This case study introduces measurements of turbulent fluxes in a nocturnal boundary layer in North Germany with the new helicopter-borne turbulence measurement system HELIPOD, a detailed data analysis and examination in regard of systematic errors of the instrument, and some comparison with local similarity theory and experiments of the past, in order to confirm the occurrence of small vertical turbulent fluxes. The examined nocturnal boundary layer offered excellent conditions to analyse the quality of the measurement system. In this connection, a detailed look at a strong ground-based inversion disclosed small turbulent fluxes with a spectral maximum at ten metres wavelength or less, embedded in intermittent turbulence. For verification of these fluxes, the measurements were compared with well established results from past experiments. Local similarity theory was applied to calculate dimensionless variances of the turbulent quantities, which were found in good agreement with other observations. Since shear and stratification varied significantly on the horizontal flight legs due to global intermittency, a method was developed to determine vertical gradients on a horizontal flight pattern, by use of small fluctuations of the measurement height. With these locally determined gradients, the gradient transport theory became applicable and the turbulent diffusivities for heat and momentum, the Richardson number, and the flux Richardson number were estimated within isolated strong turbulent outbursts. Within these outbursts the flux Richardson number was found between 0.1 and 0.2. The functional relationship between the gradient Richardson number and the turbulent Prandtl number agreed well with observations in past experiments and large eddy simulation. The impact of the stratification on the vertical turbulent exchange, as already described for the surface layer using Monin-Obukhov similarity, was analogously observed in the very stably stratified bulk flow when local scaling was applied.

Keywords: Nocturnal boundary layer, Very stably stratified flow, Intermittent turbulence, Airborne flux measurements, HELIPOD, Local similarity theory

1. Introduction

Turbulent transport in the nocturnal boundary layer and especially in the very stable stratified nocturnal ground-based inversion is of considerable practical importance, regarding for instance pollutant dispersion or flux parameterization in numerical atmospheric models (e.g., Beljaars and Holtslag, 1991). Many attempts have been made to develop theories and numerical models describing this kind of atmospheric flow, but the formulation of turbulence within the very stably stratified

boundary layer is difficult and uncertain (Nieuwstadt, 1984b; Garratt et al., 1996; Mahrt, 1998). Compared to the convective boundary layer, the very stable boundary layer is hardly understood, mainly because of the multiplicity of physical processes that govern stable flow (e.g., Mahrt, 1985; Lenschow et al., 1988; Smedman, 1988; Smedman, 1991; Yagüe and Cano, 1994) and in particular due to the suppression of vertical transport which results in intermittent turbulence, non-stationarity, inhomogeneity, and a disconnection from the ground surface (e.g., Dias et al., 1995; Mahrt, 1998). Most of the numerical models, including recent large eddy simulations (LES), concentrate on the weakly stable boundary layer, characterized by homogeneous turbulence, and uniform stratification and shear (e.g., Andrén, 1995; Schumann and Gerz, 1995). In the interior of a very stable boundary layer many of the transporting eddies, which may be organized in thin layers or short lived bursts, are not resolved by the model grid. This sub-grid turbulence is parameterized by sub-grid-scale (SGS) models. Experimental data for testing the SGS models in the very stable case, especially above the surface layer, are rare (Nieuwstadt, 1984b; Mahrt, 1998).

The very stable boundary layer over a flat surface is normally characterized by weak winds, and weak and intermittent turbulence (e.g., Wittich, 1991). The measurement accuracy of second-order statistics like turbulent fluxes is therefore limited by the prohibitively long averaging time required (e.g., André and Mahrt, 1982) when measured with ground based instruments like masts. For example, mast measurements in a flow with typical mean wind speed take more than half an hour to obtain a 10 km fetch (in order to achieve significant statistics). During this time external conditions, like net radiative surface cooling, the height of the boundary layer and elevated layers of strong shear, or the direction and magnitude of a low level jet, may already change significantly. Airborne measurement systems cover the same distance in less than five minutes. The influence of non-stationarity on the measured time series is therefore much smaller compared to ground based measurements. Aircraft measurements deliver more or less a snapshot of the flow and allow therefore an analysis of its horizontal variability.

Since the turbulent structures in a very stably stratified flow are usually very small, the size of the eddies responsible for the major part of the vertical turbulent transport might be of the order of metres. Fast responding measurement instruments are essential in order to resolve the spectral range that contains most of the turbulent energy, and to avoid systematic errors of the vertical turbulent fluxes due to finite sampling rates.

Furthermore, an instrument is required that has minimum influence on the interesting spatial scale of the flow upstream of the sensors.

In general, the geometric dimensions of the airborne body containing the sensors should be smaller than the eddies of interest, and the sensors should be far away from any sources of artificial eddies like rotors. A common airplane strongly disturbs the atmospheric flow by its large fuselage diameter, the wings, and the engines. Therefore, most research airplanes are equipped with nose booms containing the sensors. Unfortunately, this solution incorporates the disadvantages of nose boom oscillations, organ pipe effects, and a large separation between the location of the sensors and the navigation system. Since the length of the nose boom is mechanically limited, the flow at the tip of the nose boom is still altered by the airplane. The influence of the geometry and the engines of research airplanes on the measurements and the possibility of an on-line correction are the subject of the new Special Research Program No. 420 'Flight Measurement Technique' of the German Science Foundation. An alternative to airplanes, and possibly a better solution for measurements especially in the stable boundary layer, is the helicopter-borne sensor package HELIPOD (see next section), which combines highly resolving sensors and navigation systems closely packed in the tip of a small container (about half a metre diameter) hanging outside the down-wash area of the helicopter rotor. Besides, for measurements in a ground-based inversion, which is usually rather shallow, it is often much easier, with regard to flight safety and rules, to operate a helicopter than an airplane over land.

Last but not least a careful analysis of the measured time series, especially in the frequency domain, is necessary to distinguish real vertical turbulent fluxes from artifacts caused by natural modes of the system and vertical movements of a vehicle in a boundary-layer flow that is characterized by large vertical gradients.

In this case study we introduce measurements of turbulent fluxes in a nocturnal boundary layer with the new helicopter-borne turbulence measurement system HELIPOD and present a detailed data analysis in regard of systematic errors of the instrument. The results are compared with local similarity theory, numerical models, and other field experiments, in order to verify the observed small vertical turbulent fluxes.

2. Measurement System

The data presented here were collected during the first field campaign over land-surface with the recently developed helicopter-borne high-resolution turbulence measurement system HELIPOD. The HELIPOD is an autonomously operating sensor package, constructed to be carried

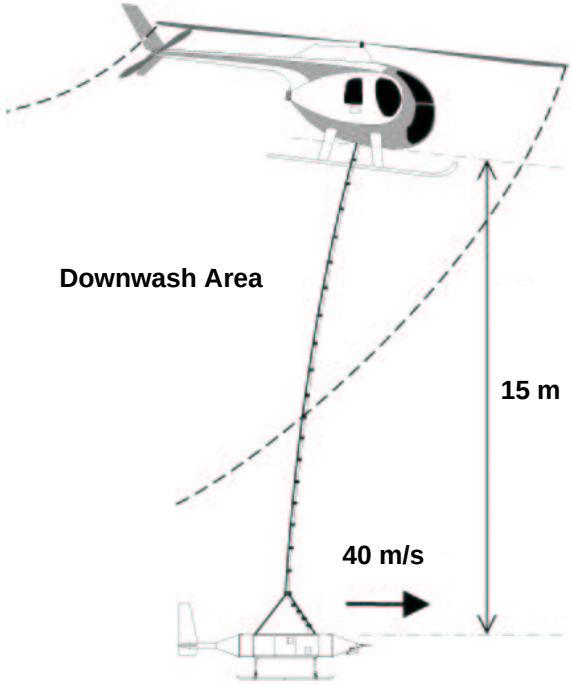

Figure 1. Sensor package HELIPOD with helicopter (from a drawing by C. Wode - personal communication).

by almost any helicopter on a rope of 15 m length at a typical ground speed of 40 ms^{-1} (Figure 1). Studies of the Institute for Flight Mechanics at the Technical University of Braunschweig (Germany) have shown that this configuration ensures measurements without or with negligible distortion due to the down-wash of the helicopter (Büchler, 1993; Wode and Roth, 1996). In the following analysis the influence of the rotor blades was identified as sharp peaks at the high frequency end of the co-spectra (see Section 5), which did not contribute to the measured fluxes. The HELIPOD itself is a container of about 5 m in length, 0.5 m in diameter, and 250 kg in weight. It carries its own navigation systems, power supply, data storage, and fast responding sensor equipment, especially designed for *in situ* measurements of the turbulent fluctuations of wind, temperature, humidity, and the turbulent fluxes.

To achieve a high temporal resolution, HELIPOD measures each meteorological parameter with at least two different types of instruments (see also Muschinski and Wode, 1998): one that has a short response time, but the disadvantage of a temporal drift. These sensors are sampled at 100 to 1000 Hz internally. The other type of sensors

respond slowly but have a high accuracy on a large time scale; these data are stored at 20 Hz. To achieve a large frequency range, the data sets are united by complementary filters. The results are 100 Hz time series of the meteorological parameters, equivalent to one measurement point every 40 cm.

In detail the HELIPOD is equipped (see also Wode et al., 1996; Schürmann and Wode, 1996) with a five-hole-probe, an inertial navigation system (INS), and two GPS systems, to determine the static pressure, the true air speed, the position, and the attitude of the system, and finally the wind vector. The navigation systems are complemented by a radar altimeter. Temperature is measured by a conventional Rosemount resistance thermometer and a fast wire element. For humidity measurements the HELIPOD is equipped with a Lyman Alpha hygrometer, a capacitive sensor (humicap), and a dew point mirror.

3. Experimental set-up

The experimental site was located in the nature reserve Drömling in North Germany, about 24 km east of the city of Braunschweig (Figure 2). The investigation area was of nearly square shape with sides of about 11 km length. The area featured a very flat topography (changes less than 5 m), combined with sparse settlement, few trees, reaped fields, and a lot of fallow land. It was chosen in order to minimize topographic effects on the turbulence measurements within the boundary layer.

Two-hour-flights with the HELIPOD during the field experiment DREX (Drömling Experiment) were carried out in the nocturnal boundary layer with a Bo-105 helicopter on 18 and 19 August, 1995, beginning at 4:00 UTC, right after sunrise. During that week North Germany was near the centre of a summer anti-cyclone. Dry air was carried from the East into the investigation area at low wind speeds. The afternoons before the experiments had well developed convective boundary layers. Since no clouds appeared during the night, radiational cooling was strong, and a strong ground-based inversion developed.

Figure 3 shows the vertical profiles of potential temperature, measured by radio sondes launched from the centre of the experimental site in the morning of both measurement days: Between 03:00 UTC and at least 06:00 UTC a ground-based inversion of $5-6\times10^{-2}$ Km^{-1} reached a height of 200 m above ground level. Above the ground-based inversion, the neutrally stratified residual layer of the convective boundary layer of the afternoon before reached about 2000 m height, ending in a capping inversion. The wind profiles near the surface are shown for both days in Figure 4: On 18 August only data from three radio

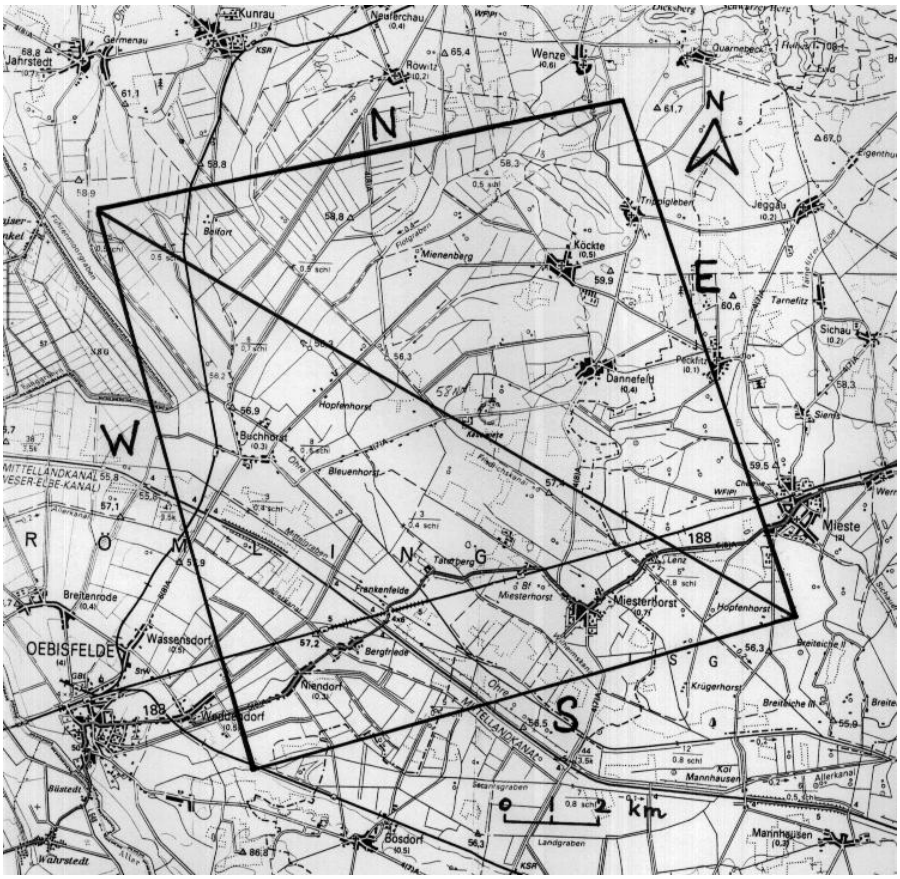

Figure 2. Map of the investigation area within the nature reserve Drömling. Also drawn in are the four flight legs S, W, N, E, and the diagonal leg flown on 18 August.

sondes before, during, and after the HELIPOD flight were available. The profiles show a low level jet with a wind maximum between 4 and 8 ms^{-1} on the top of the ground-based temperature inversion. Also the wind direction varied between 30 and 120 degrees. Such variation of the nocturnal inertial oscillations were treated by Jacobi and Roth (1995). On the second day no low level jet developed, but a layer of strong wind shear between 100 and 150 m above ground was detected during a HELIPOD vertical sounding at 4:00 UTC, right before the horizontal flight pattern started. Since this layer was not observed by the radio soundings, the life time of this layer of strong shear was assumed to be very short.

To measure the turbulent fluxes within the nocturnal boundary layer, two similar flights were performed: On 18 August, a square pattern with 11 km legs and a diagonal leg (Figure 2) was flown in the

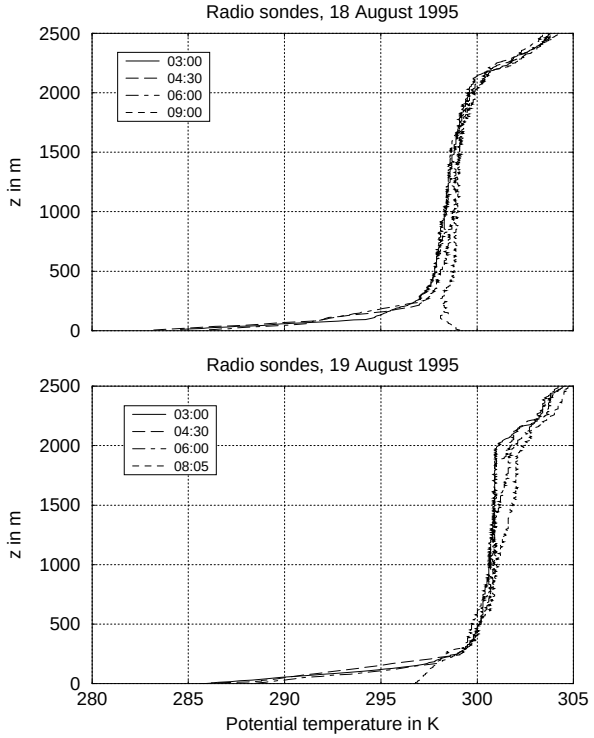

Figure 3. The potential temperature, θ versus height, z above ground level, as measured by radio soundings in the mornings of 18 and 19 August. On both days, beginning at 03:00 UTC, one hour before the HELIPOD flights, four radio sondes were launched.

middle of the ground-based inversion (height above ground $z = 100$ m) and in the residual layer ($z = 370$ m). One pattern took about 40 min. The next day, the same square pattern without the diagonal was flown again in the middle of the inversion ($z = 100$ m), at its top ($z = 190$ m), and in the residual layer ($z = 450$ m). This kind of pattern took about 25 min. For meteorological examinations only the straight flight legs were useful. The turns at the corners of the flight pattern were cut out of the time series.

4. Spectral analysis of the measured data

On both days the nocturnal boundary layer was characterized by weakly turbulent flows. The ground-based inversion contained sufficient mechanical shear, but vertical motion was strongly suppressed by stable thermal stratification. The residual layer lacked the necessary shear

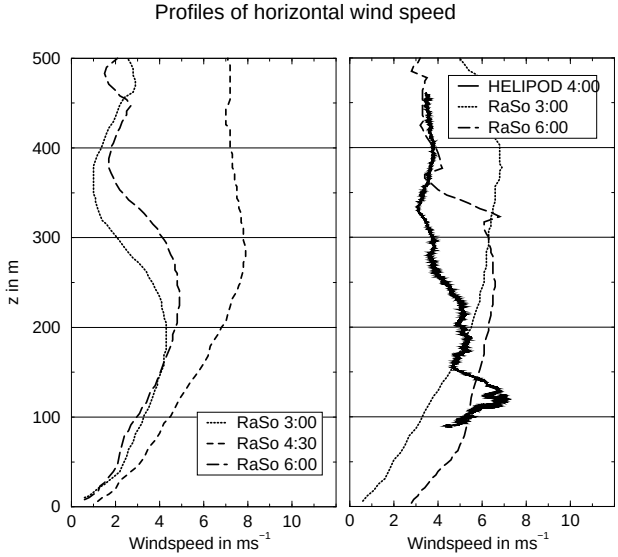

Figure 4. Vertical profiles of wind speed measured on both days by radio sondes (RaSo) and HELIPOD. On 18 August (left side) only radio sonde data were available. The 4:30 UTC radio sonde on 19 August (right side) supplied no wind data.

to develop a strongly turbulent flow. The measurement flights with the HELIPOD therefore yielded time series of meteorological parameters with a comparatively weak influence of turbulence, especially in comparison to measurements in a convective boundary layer. Hence it was possible to distinguish plainly the systematic errors and normal modes of the system (actually this was the initial intention of the field experiment).

The most important normal mode of the HELIPOD was caused by a harmonic oscillation of the container under the helicopter at the end of the rope of $l = 15$ m length. Using the simple model of a plane (mathematical) pendulum, the harmonic period came to

$$D_p = 2\pi\sqrt{\frac{l}{g}} \approx 7.8 \text{ s}, \tag{1}$$

with acceleration g due to gravity. Together with a mean ground speed of $c = 40$ ms^{-1} this led to a pendulum wavelength of 312 m or wavenumber $k_p = 2 \cdot 10^{-2}$ m^{-1}, using the wavenumber definition

$$k_p = \frac{2\pi}{c \cdot D_p}. \tag{2}$$

The pendulum oscillations caused small vertical harmonic movements of the system with amplitudes between 0.5 and 1 m that were modu-

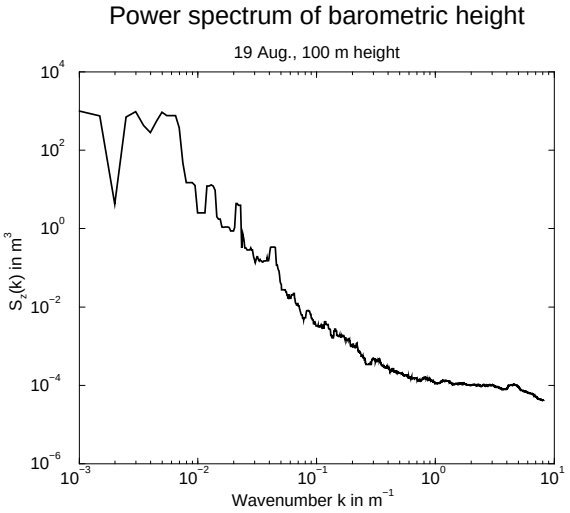

Figure 5. Power spectra $S(k)$ of the barometric height measured by the HELIPOD on a horizontal flight leg. The spectral density was smoothed by a moving average over 0.1 decade width on a logarithmic wavenumber axis.

lated on the slower fluctuations of the flight level (see first time series in Figure 8). They can be identified in the spectrum of barometric height (Figure 5) at 0.5 k_p, k_p, and 2 k_p. The occurrence of the first harmonic (2 k_p) is not surprising since the height passed through two complete oscillations during each pendulum period. The second important normal mode is the bank oscillation with $D_b \approx 1$ s or wavenumber $k_b = 0.17$ m^{-1}, round the longitudinal axis of the HELIPOD.

To identify these normal modes in the measured time series, power spectra of temperature T, vertical wind w, and the horizontal wind components u (in mean wind direction) and v (perpendicular to the mean wind) were calculated for each flight leg, using a fast Fourier transformation (FFT). Their weighted spectral densities $k \cdot S(k)$ were smoothed by a moving average over 0.1 decade width on a logarithmic wavenumber axis (Figures 6 and 7).

The normal modes of the HELIPOD at wavenumbers k_p and k_b, and also the first and second harmonic of the pendulum oscillation can be easily identified in the velocity spectra of the measurements in the neutrally stratified residual layer (Figure 6), while they were largely lost in by the signal of atmospheric turbulence in the ground-based inversion (Figure 7). The temperature spectrum exhibits only the pendulum oscillation at k_p in stable stratification. The large contributions to the small wavenumbers ($k < 10^{-2}$ m^{-1}), especially in the ground-

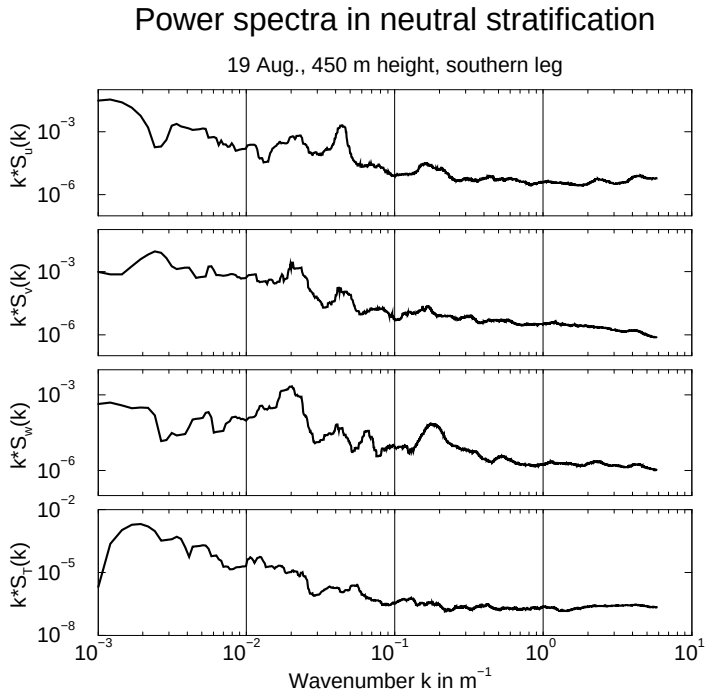

Figure 6. Power spectra $S(k)$ (weighted with wavenumber k) of all three wind components and temperature (in m^2s^{-2} and K^2, respectively), measured at 450 m height in the residual layer on the southern leg of 19 August.

based inversion with its large vertical gradients, were caused by slow vertical movements of the whole system (HELIPOD-helicopter).

For further analysis a set of time series measured on a 11 km horizontal flight leg is displayed in Figure 8: The barometric height z varied slowly between 160 and 130 m on this leg. Also the pendulum oscillations can be identified. The potential temperature θ and the wind component u were strongly correlated with the slow fluctuations of height z, in agreement with the vertical profiles in Figures 3 and 4. This correlation can also be identified in the wind component v, while the vertical wind w seemed to be largely uncorrelated to the slow changes of height. Nevertheless, the time series of vertical wind featured the pendulum oscillations with $D_p \approx 8$ s, and also the oscillations in u and v had amplitudes that were too large compared with the small pendulum oscillations in height z. The source of this artifact was an inadequate calibration of the system: The pendulum movements of the HELIPOD were not completely eliminated from the five-hole-probe measurements, although extensive testing and in-flight calibration of the system were

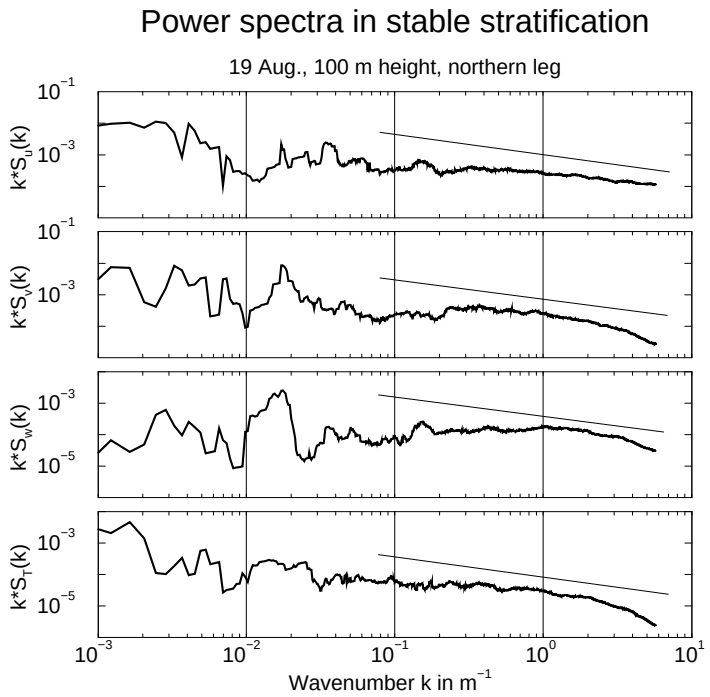

Figure 7. Power spectra $S(k)$ (weighted with wavenumber k) of all three wind components and temperature (in m^2s^{-2} and K^2, respectively), measured at 100 m height in the ground-based inversion on the southern leg of 19 August. For comparison a Kolmogorov $k^{-5/3}$ law (appearing as a straight line proportional to $k^{-2/3}$) is added at the small scale end.

performed before the field experiment. The following sections will show that this defect did not affect the quality of the flux measurements.

In concluding this section the data collected in the ground-based inversion are compared with the theory of isotropic turbulence. The straight lines in the spectra of Figure 7 represent a Kolmogorov $k^{-5/3}$ law (which appears in the $k \cdot S(k)$ plot as a $k^{-2/3}$ law). At the small scale end the spectral densities exhibit a power law close to $k^{-5/3}$, beginning at wavenumbers between 0.3 m^{-1} (for u, v, and T) and 1 m^{-1} (for w), respectively. Most of the horizontal turbulent motion was therefore distributed at wavelengths around 20 m, while isotropic turbulence probably started at about 6 m wavelength, which is plausible since the strong thermal stratification of the ground-based inversion suppressed large scale vertical motion.

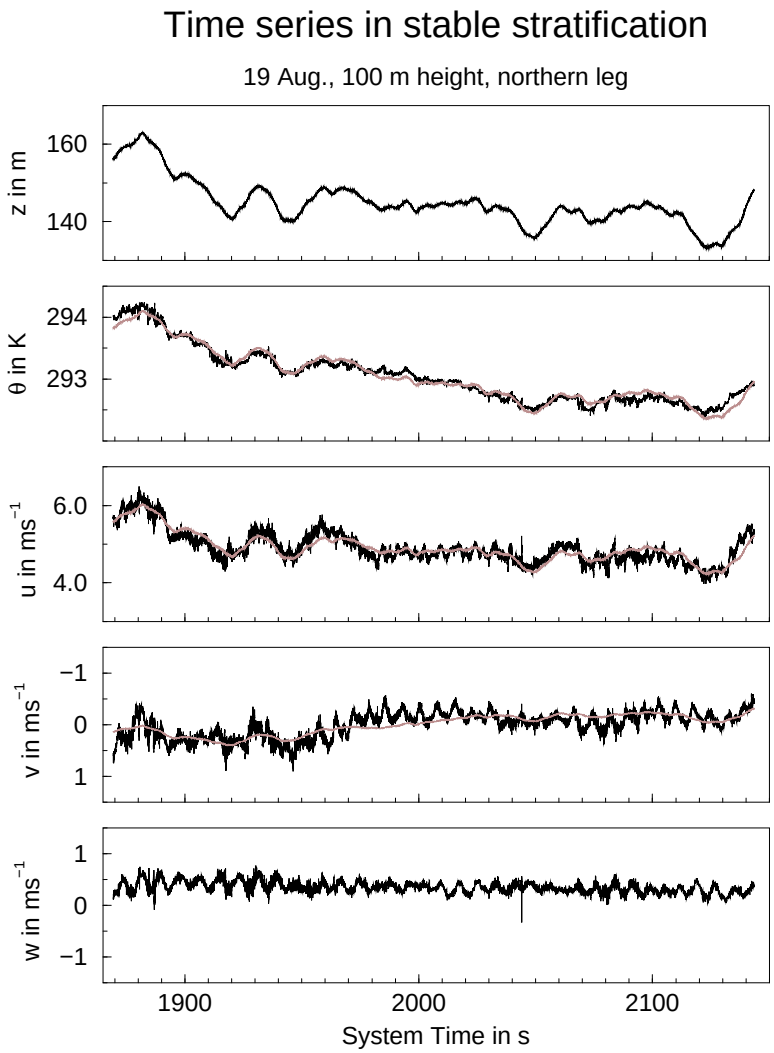

Figure 8. Time series of barometric height, potential temperature, and wind components measured on a 11 km leg in stable stratification. The results of the inverse modelling are added to the θ, u, and v series (grey line).

5. Turbulent fluxes

Before calculating the vertical turbulent fluxes of sensible heat (H) and momentum (τ), the contributions of the HELIPOD oscillations to the fluxes had to be examined. For this purpose, the co-spectra of potential temperature θ and wind components u and v with the vertical wind

speed w

$$C_{w\phi}(k) = Re\left\{\int d\xi\ \rho_{w\phi}(\xi)\ \mathrm{e}^{ik\xi}\right\}\ , \tag{3}$$

(with cross-correlation function ρ, a separation ξ between two measurement points on the flight leg, and $\phi = u, v, \theta$) were calculated and analysed on each leg. The co-spectra represent the spectral distribution of the flux, while the integral of a co-spectrum gives the flux itself. Since the vertical fluxes in the residual layer were expected to be zero (e.g., Stull, 1988), the co-spectra were calculated from time series measured in the ground-based inversion (Figure 9), in order to compare the amplitude and spectral location of the expected turbulent fluxes with the virtual contributions due to vertical oscillations of the HELIPOD. Slow variations in flight height of the whole system gave large positive and negative contributions to the spectral density at the large scale end ($k < 10^{-2}$ m^{-1}). In the centre region, at wavenumbers smaller than $5 \cdot 10^{-2}$ m^{-1}, the pendulum oscillation and also its first harmonic are clearly displayed by large peaks. The bank oscillation can be identified at $k_b = 0.17$ m^{-1}, but its shallow peak is already obscured by the turbulent signal which starts gradually at approximately $k = 0.1$ m^{-1}. The influence of the rotor blades of the helicopter is visible as very sharp peaks (which therefore do not contribute to the fluxes) at $k = 3.7$ m^{-1} and $k = 5.8$ m^{-1}. They cannot be seen in the power spectra in Figures 6 and 7, because they were removed by the smoothing procedure.

After this examination of the co-spectra it was obvious that the virtual contributions of the HELIPOD oscillations and height fluctuations at the large scales were enormous compared to the small turbulent fluxes in the very stably stratified flow and that they had to be removed. The demands on the following high pass filter routine were: 1) to cut off the virtual contributions, but 2) to leave the actual turbulent fluxes untouched. This was achieved by using a numerical filter described by Schlittgen and Streitberg (1994) and defined by a sequence of weights

$$W_j \propto \frac{\sin\left(2\pi j \frac{f_C}{f_S}\right)}{j} \cdot \frac{2n+1}{2\pi j} \cdot \sin\left(\frac{2\pi j}{2n+1}\right)\ , \quad -n \le j \le n \tag{4}$$

with a central weight

$$W_0 \propto 2\pi\, \frac{f_c}{f_S}\ , \tag{5}$$

representing a finite numerical window with $2n + 1 = 1415$ elements that moved over the time series which were sampled at $f_S = 100$ Hz.

The shape of the Fourier transformed function of Equation 4 looks very much like a rectangle (see first part of the function), i.e. the edge of

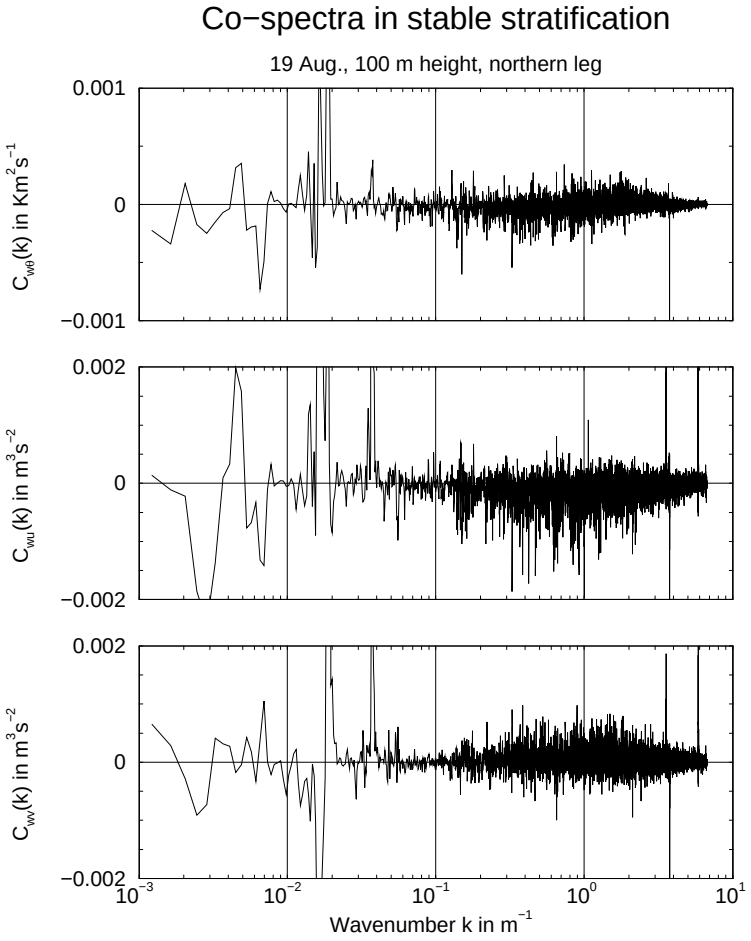

Figure 9. Co-spectra of potential temperature θ and the horizontal wind components u and v with the vertical wind speed w, representing the spectra distribution of the vertical fluxes of heat and momentum. The time series were measured within the ground-based inversion at 100 m height, on the northern leg of 19 August.

the filter in the frequency domain is very steep. The Gibbs' phenomenon (due to finite size of the window) is largely reduced by the second and third part of Equation 4. For a picture of the transfer function see Schlittgen and Streitberg (1994). The impact of the filter routine on the turbulent fluxes is illustrated by the C_{wu} co-spectrum in Figure 10. Choosing the cut off wavenumber $k_C = 7 \cdot 10^{-2}$ m^{-1} (corresponding to the frequency $f_C = 0.45$ Hz) between the first harmonic of the pendulum oscillation and the onset of the turbulent flux made sure that the turbulent part of the co-spectrum was still recorded while the virtual

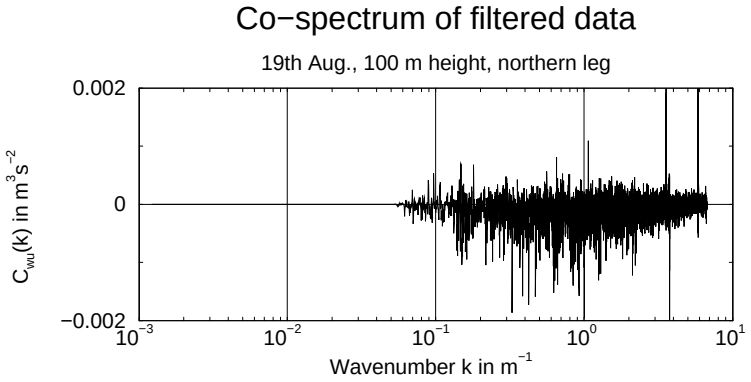

Figure 10. Co-spectra of wind component u with the vertical wind speed w calculated with high pass filtered data. The spectrum contains the entire band width (starting at $10^{-3}\mathrm{m}^{-1}$). All contributions of scales larger than $5 \cdot 10^{-2}\mathrm{m}^{-1}$ were suppressed by the filter routine.

contributions by the HELIPOD oscillations were excluded (compare Figure 10 with the central graph in Figure 9), with the exception of the bank oscillations at k_b. Since the contributions to the co-spectra of the latter were located on a small spectral band with a comparatively small amplitude, the error in the following flux calculation due to the bank oscillations was for certain in the order of a few per cent only.

The vertical turbulent flux of sensible heat H and the total vertical turbulent flux of horizontal momentum τ were calculated from the high pass filtered time series of each flight leg, using the conventional eddy correlation method:

$$H = \varrho\, c_p \,\langle w'\theta' \rangle_P \tag{6}$$

$$\tau = \varrho \sqrt{\langle w'u' \rangle_P^2 + \langle v'u' \rangle_P^2} \tag{7}$$

(e.g., Stull, 1988), with air density ϱ and specific heat c_p of air. The brackets indicate the average over all measurement points on one flight leg P of 11 km length, the prime indicates high pass filtered time series. Since the meteorological characteristics of the two measurement days were quite similar, the results of both days are depicted together in one diagram in Figure 11 as a function of height z above the ground. The error bars were calculated corresponding to the method introduced by Lumley and Panofsky (1964), and Lenschow and Stankov (1986). The statistical error ΔH of the vertical turbulent heat flux H due to finite length P is defined by

$$\Delta H = \varrho\, c_p \sqrt{2\,\frac{I_H}{P}\,\left[\langle w'^2 \rangle_P \,\langle \theta'^2 \rangle_P \;+\; \langle w'\theta' \rangle_P^2\right]}\,, \tag{8}$$

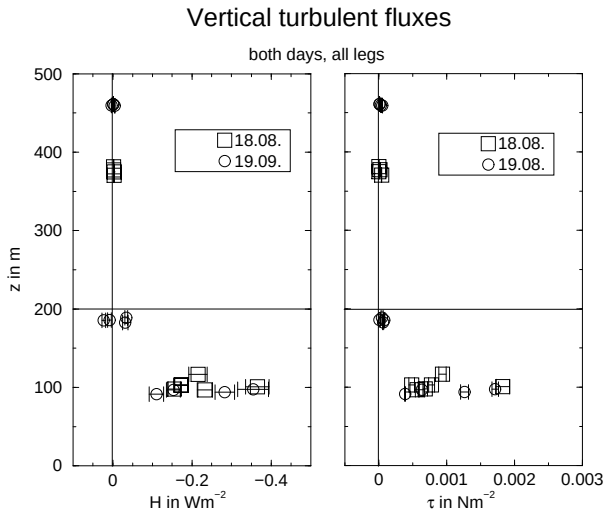

Figure 11. Vertical profiles of the vertical turbulent flux of sensible heat H and the total vertical turbulent flux of horizontal momentum τ, calculated from the measured time series of each flight leg on both measurement days. The horizontal lines at $z =$ 200 m above the ground indicate the height of the ground-based inversion. The error bars represent the statistical errors ΔH and $\Delta\tau$ calculated with the method of Lenschow and Stankov (1986).

with the integral length scale of vertical turbulent heat flux

$$I_H = \frac{1}{2} \cdot \int_{\xi_1}^{\xi_2} d\xi \; \rho_{w\theta}(\xi) \; . \tag{9}$$

The parameters ξ_1 and ξ_2 indicate the first positive and negative separation ξ, where the cross-correlation $\rho(\xi)$ becomes zero. The error $\Delta\tau$ of the vertical momentum flux τ was calculated accordingly. Due to the small scale of turbulence in the nocturnal boundary layer, these errors were rather small. In regard of this test, the flight legs were of sufficient length to measure the vertical fluxes with high significance.

In keeping with the theory of the nocturnal boundary layer (e.g., Stull, 1988), the vertical fluxes vanished above the ground-based inversion ($z > 200$ m; Figure 11): The measured heat fluxes within the residual layer were smaller than 0.01 Wm^{-2}, the momentum fluxes were smaller than 10^{-4} Nm^{-2}. This demonstrates that the system HELIPOD detected the vertical fluxes of heat and momentum without significant offset from zero. The flight measurements near 100 m height resulted in a mean downward heat flux $\bar{H}$ of 0.23 Wm^{-2} for both days with a standard deviation of 0.1 Wm^{-2}, which was compatible with

Table I. Mean vertical turbulent fluxes (averaged over all legs of the same height and day).

Date	$\bar{z}$ in m	$\bar{H}$ in Wm^{-2}	$\bar{\tau}$ in 10^{-3} Nm^{-2}
18.08	102	-0.228 ± 0.083	0.96 ± 0.51
	376	-0.003 ± 0.001	0.02 ± 0.02
19.08	95	-0.225 ± 0.113	1.00 ± 0.60
	186	-0.008 ± 0.029	0.05 ± 0.03
	460	-0.001 ± 0.003	0.03 ± 0.02

the strongly stable stratification. The results for the momentum flux τ scattered between 0.3 and $1.8 \cdot 10^{-3}$ Nm^{-2}, their mean value was $1.0 \cdot 10^{-3}$ Nm^{-2}. The mean fluxes and their standard deviations are also listed in Table I.

6. Discussion

The main problem with these remarkably small vertical turbulent fluxes, measured on HELIPOD flights in a well-developed nocturnal ground-based inversion, is the lack of any other measurements or model data that could support the introduced results. The situation becomes even more complicated since the HELIPOD is a new and, to the scientific community, largely unknown measurement system, using an unusual method and requires therefore an unusual handling of the measured data, particularly in regard of its normal modes, which are totally different from those known from conventional measurement airplanes, like the nose boom oscillations or the so-called organ-pipe effect. To increase the trust in the measurements within the ground-based inversion, we will compare them with theory and other measurement results found in the literature. The most obvious opportunity to prove our measured data in general is the application of local similarity theory (Nieuwstadt, 1984b), in order to see whether the fluxes and other turbulent parameters of the examined stable boundary layer meet theory and measurements from the past. In the second part of the discussion the measured fluxes themselves are examined indirectly by calculation of the turbulent exchange coefficients.

6.1. Local scaling

For inter-comparison of stably stratified turbulent flows, measured at different places, under different stratification strengths, and at different heights above the ground (and above the surface layer, so that the turbulent fluxes are expected to be significantly different from the surface fluxes and become height dependent), the dimensionless presentation of the variances and covariances of the meteorological parameters using local scaling is appropriate. In a ground-based inversion of height h, the turbulent flow above $z = 0.1\,h$ (Nieuwstadt, 1984a) depends mainly on the height z and the local values of the turbulent fluxes $H(z)$ and $\tau(z)$ (Nieuwstadt, 1984b; Holtslag and Nieuwstadt, 1986). Similar to Monin-Obukhov similarity theory, the local scales of wind speed, temperature, and height are defined by

$$u_L^2(z) \;=\; \frac{\tau(z)}{\varrho} \tag{10}$$

$$\theta_L(z) \;=\; -\frac{H(z)}{\varrho\, c_p \cdot u_L(z)} \tag{11}$$

$$L_L(z) \;=\; \frac{\bar{\theta} \cdot u_L^2(z)}{\kappa\, g \cdot \theta_L(z)}\,, \tag{12}$$

with von-Kármán's constant $\kappa = 0.4$. The over-bar indicates mean values at height z. The local scales measured on the horizontal flight legs within the ground inversion on both days are listed in Table II and Table III, together with the flux Richardson number (e.g., Garratt, 1992)

$$\mathrm{Ri_f} = \frac{g}{\bar{\theta}} \cdot \frac{\langle w'\theta' \rangle}{\langle w'u' \rangle\, \partial_z \bar{u} \;+\; \langle w'v' \rangle\, \partial_z \bar{v}} \quad . \tag{13}$$

(using the abbreviation $\partial_z \equiv \frac{\partial}{\partial z}$), which describes the ratio of buoyancy forces to mechanical shear. The vertical gradients were estimated from the wind profiles in Figure 4. The local scales were used to calculate the dimensionless local height z/L_L and the dimensionless values of the standard deviations σ_ϕ of the turbulent quantities $\phi = u, v, w, \theta$, which should be constant with respect to height and stability (Rogers et al., 1995). The results are listed in Table IV, together with the dimensionless standard deviations measured during other field campaigns in a stable boundary layer: namely, mast measurements in Cabauw/Netherlands (Nieuwstadt, 1984b; Sorbjan, 1987) and Boulder/Colorado (Sorbjan, 1987), the Minnesota-Experiment 1973 (Caughey et al., 1979; Sorbjan, 1986; Sorbjan, 1987), and the aircraft field experiments SESAME 1979 in Oklahoma (Sorbjan, 1988) and IBLEX 1990 over the Irish Sea (Rogers et al., 1995). Table IV shows

Table II. Local scales, local height, and flux Richardson number of the ground-based inversion on 18 August.

Leg	South	East	North	West	diagonal
Height in m	116.7	96.6	100.6	102.9	97.8
u_L in 10^{-2} ms^{-1}	2.74	2.12	3.83	2.46	2.34
θ_L in 10^{-3} K	6.24	8.71	7.59	5.51	5.27
L_L in m	8.90	3.82	14.24	8.36	7.69
z/L_L	13.12	25.29	7.06	12.30	12.72
$\mathrm{Ri_f}$	0.34	0.65	0.37	0.51	0.33

Table III. Local scales, local height, and flux Richardson number of the ground-based inversion on 19 August.

Leg	South	East	North	West
Height in m	96.7	97.5	93.8	91.4
u_L in 10^{-2} ms^{-1}	2.26	3.71	3.18	1.76
θ_L in 10^{-3} K	5.39	7.61	7.07	4.97
L_L in m	6.99	13.34	10.58	4.61
z/L_L	13.83	7.31	8.87	19.81
$\mathrm{Ri_f}$	0.10	0.18	0.10	-

that the dimensionless standard deviations calculated from HELIPOD measurements are very similar to those obtained from other experiments in the stable boundary layer. Especially the agreement with the IBLEX data measured in a marine atmospheric boundary layer, which was much less stably stratified than the ground-based inversion over Drömling, is remarkable.

Due to the strong temperature gradient the downward turbulent heat flux H in the ground-based inversion was limited by buoyancy constraints. Turbulence was largely suppressed, which is also expressed by large values of the local height z/L_L (Mahrt, 1998) in Table II and Table III.

Though the turbulence at flight levels $z \approx 100$ m height was not completely suppressed but intermittent: the wind profiles on 18 August in Figure 4 show a low level jet on top of the ground-based inversion. This produced enough shear near $z = 100$ m to provide a small flux Richardson number $\mathrm{Ri_f} < 0.7$ (Table II) and turbulent outbursts in the stably stratified flow, similar to observations of Smedman (1988).

Table IV. Local scales and dimensionless standard deviations measured by HELIPOD and averaged over all legs each day (18 Aug., 19 Aug.). For comparison the table lists the results of other field experiments in the stable boundary layer: Cabauw (Cab.), Boulder (BAO), the Minnesota-experiment (Minn.), SESAME, and IBLEX. The measurements near Boulder (BAO) and during SESAME were performed on different days and with various stratification strengths. The standard deviation of the horizontal wind is defined by $\sigma_h^2 = \sigma_u^2 + \sigma_v^2$.

	18 Aug.	19 Aug.	Cab.	BAO	Minn.	SESAME	IBLEX
L_L in m	8.60 ± 3.73	8.88 ± 3.86	-	0.3 - 133	-	63 - 447	304 ± 219
u_L in 10^{-2} ms^{-1}	2.70 ± 0.67	2.72 ± 0.88	-	1 - 24	-	18 - 44	26.6 ± 4.2
θ_L in 10^{-3} K	6.66 ± 1.46	6.26 ± 1.27	-	23 - 120	-	21 - 44	19.2 ± 4.4
σ_u/u_L	2.09 ± 0.35	2.54 ± 0.41	2.6	-	2.4	2.0	2.01 ± 0.12
σ_v/u_L	2.25 ± 0.38	2.47 ± 0.50	-	-	1.8	2.12	2.44 ± 0.17
σ_h/u_L	3.07 ± 0.52	3.54 ± 0.65	-	4	3.0	2.9	3.16 ± 0.21
σ_w/u_L	1.47 ± 0.18	1.72 ± 0.18	1.5	2	1.6	1.73	1.43 ± 0.08
σ_θ/θ_L	4.82 ± 1.44	5.99 ± 1.47	3.5	4	2.4	1.73	4.74 ± 1.04

On 19 August, the wind-profile in Figure 4, which was measured on a vertical sounding by the HELIPOD immediately before the horizontal flight pattern at $z \approx 100$ m started, shows a short lived elevated layer of strong shear at about 100 m, which may be compared with the observations of Mahrt (1985). Actually, on most of the flight legs within the ground-based inversion only intermittent turbulence, in the sense of *global intermittency* (Mahrt, 1989), was found, in keeping with the observations of Holtslag and Nieuwstadt (1986), who found only non-continuous turbulence for $h/L_L > 6$. While on the first day, on all five flight legs in the inversion below the low level jet, clearly intermittent turbulence was observed, the situation on the second day was something less simple. Figure 12 displays the time series of turbulent kinetic energy

$$E(t) = \frac{1}{2}\left(u'^2 + v'^2 + w'^2\right) \ , \tag{14}$$

measured in the inversion on the second day, in chronological order: The first two legs were characterized by an intermittent turbulent flow with turbulent outbursts covering about one fifth of the measurement time at flux Richardson numbers between 0.1 and 0.2 (see Table III). On the third, northern, leg turbulence was weaker and nearly continuous with $\mathrm{Ri_f} = 0.1$ and $H = 0.3$ Wm^{-2}. The turbulent kinetic energy E was close to zero on the last, western leg. Probably the layer of strong shear vanished during the flight within the ground-based inversion and did not exist anymore when the HELIPOD reached the last flight leg. In the absence of any shear the strong thermal stratification suppressed any turbulent outbursts on the last leg.

6.2. Turbulent diffusivity

The preceding section disclosed that the turbulent energy on flight legs within the ground-based inversion was concentrated in turbulent outbursts, which were embedded in a nearly non-turbulent flow (Figure 12). A mutual comparison of time series, measured on flight legs of equal horizontal location but flown at different heights, or at the same height but on different days, and also a comparison of these time series with the topography of the measurement site, yielded no sign that the turbulent outbursts were connected to specific locations. On the contrary, the intermittency was a product of a location independent interplay between turbulence generating mechanical shear and the reduction of this shear by turbulent outbursts (Stull, 1988; Mahrt, 1998). This implies that shear and stratification were not constant over the whole flight pattern or at least over a leg, but were more or less quickly changing within the flow due to intermittency. To look in more detail

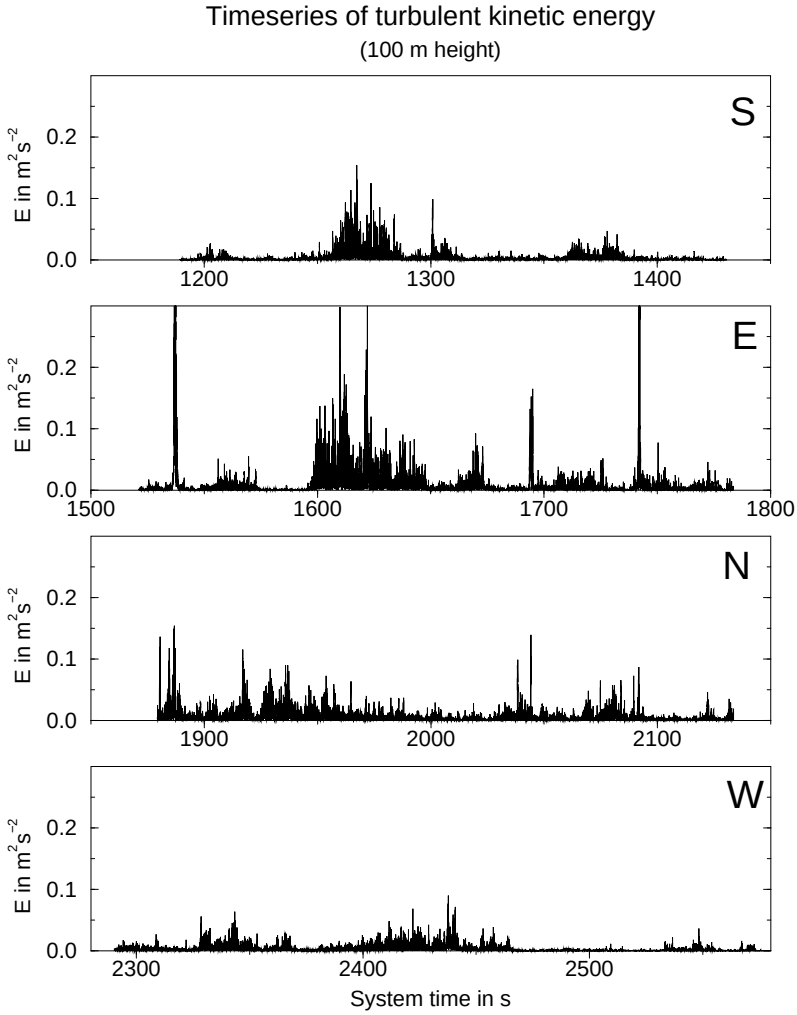

Figure 12. Time series of turbulent kinetic energy E (in chronological order), measured on all flight legs within the ground-based inversion in 100 m height on 19 August.

at the measurements in this very stably stratified flow, the parameters of those regions where most of the turbulent transport happened were determined and discussed.

First, all regions with stronger turbulence were isolated from the measured time series by 'eye'. Then those regions were selected where shear and stratification did not vary too much. The concrete criteria are explained below. The length of these regions or sub-legs was named P'. The turbulent vertical fluxes H and τ were calculated (Equation 6

and 7 with P' instead of P) and so were the local height L_L (Equation 12). Although the turbulent outbursts were rather short (P' was about 1 km), a sufficient accuracy of the fluxes could be achieved, as flux accumulation tests showed: The sub-legs of length P' were subdivided into N_f even smaller fragments of length $P'' = P' \cdot N_f^{-1}$. For each fragment P_i'' the turbulent fluxes were determined with the eddy correlation method. From these N_f results the mean fragment fluxes H_f and τ_f were calculated (e.g., heat flux):

$$H_f(N_f) = \frac{1}{N_f} \sum_{i=1}^{N_f} \langle w'\theta' \rangle_{P_i''} \,. \tag{15}$$

By variation of N_f, the fluxes H_f and τ_f became a function of sample size or integration length P'', similar to the ogives in Rogers et al. (1995), and the flux stability tests in Grossman (1984) and Grossman (1992). Figure 13 shows the result of this accumulation test applied to the strong turbulent outburst on the eastern leg of 19 August (see second diagram in Figure 12). For uniform presentation, the fragment fluxes H_f and τ_f have been normalized, i.e. divided by their 'final' values H and τ of the entire sub-leg P' (see 'h19eS1' in Table V). About 90 % of these final values were achieved after a integration length of $P'' = 60$ m. Scales larger than 100 m did not contribute to the turbulent fluxes. The flux measurements converged fast, thus the size of the turbulent patches P' was large enough to calculate representative turbulent fluxes, which is a necessary requirement for correct flux measurements.

The fluxes measured within the turbulent outbursts are listed in Table V for each sub-leg P'. While the leg-averaged values of the turbulent fluxes (see previous section) were of the order -0.2 Wm^{-2} and $1.0 \cdot 10^{-3}$ Nm^{-2}, respectively, the fluxes found in the isolated stronger outbursts reached -1.3 Wm^{-2} and $5.2 \cdot 10^{-3}$ Nm^{-2}, respectively. Nearly the entire turbulent transport took place in these outbursts, while the turbulent energy outside could almost be neglected, which is in agreement with the results of large eddy simulations in high Richardson number regions at the top of a stable boundary layer (Andrén, 1995). Figure 14 shows the impact of the thermal stratification, represented by the local stratification parameter z/L_L, on the vertical turbulent fluxes within the outbursts. With stronger stratification (larger z/L_L) the turbulent fluxes tend to zero, in good agreement with observations of Mahrt (1998). However for the strongest stratification ($z/L_L \approx 25$), observed during a short outburst on the Eastern leg on 18 August, the fluxes increased again, an effect we know no explanation for.

Table V. Vertical turbulent fluxes, vertical gradients, local height, inverse Prandtl number, flux Richardson number, and Richardson number as detected for the sub-legs.

Sub-leg	H	τ	$\partial\theta/\partial z$	$\partial u/\partial z$	$\partial v/\partial z$	L_L	Pr^{-1}	$\mathrm{Ri_f}$	Ri
	$\mathrm{Wm^{-2}}$	$10^{-3}\,\mathrm{Nm^{-2}}$	$10^{-2}\,\mathrm{Km^{-1}}$	$10^{-2}\,\mathrm{s^{-1}}$	$10^{-2}\,\mathrm{s^{-1}}$	m	1	1	1
h18s	-0.188	0.845	4.2	7.4	-1.6	8.8	0.396	0.100	0.247
h18nS1	-1.296	5.179	4.3	7.0	-4.5	19.3	0.483	0.119	0.208
h18eS1	-0.984	1.562	6.4	9.6	-1.1	4.2	0.942	0.218	0.230
h18dS1	-0.568	1.792	2.8	5.5	-0.9	9.0	0.633	0.192	0.299
h19sS1	-0.826	3.058	3.4	10.8	1.3	13.7	0.861	0.083	0.096
h19eS1	-1.356	4.948	3.9	5.7	-3.8	17.2	0.478	0.161	0.281
h19n	-0.263	1.282	3.8	6.1	-1.9	11.7	0.346	0.112	0.310
h19nM1	-0.256	1.020	3.5	6.5	-4.4	8.5	0.555	0.129	0.192
h19w	-0.096	0.394	3.5	2.5	-4.3	5.5	0.343	0.324	0.479

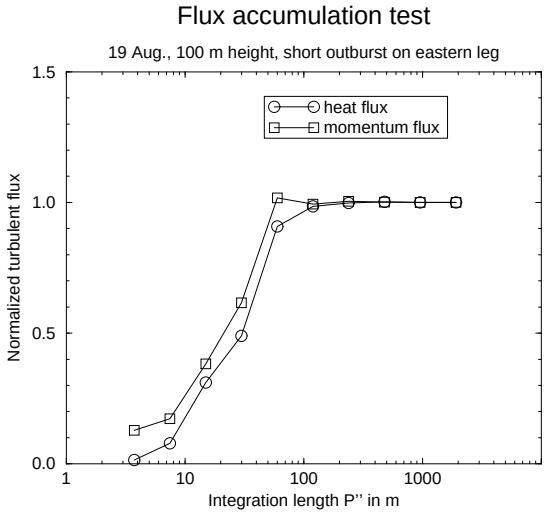

Figure 13. Flux accumulation of a turbulent outburst on the eastern leg of 19 Aug. in the ground-based inversion. The mean fragment fluxes of heat and momentum were normalized with the 'final' values of the entire outburst.

Since there was no way known to check the measured turbulent fluxes directly, neither by comparison with a theory for the very stable boundary layer, nor with numeric models, we used an indirect way via the turbulent diffusivities or transfer coefficients K_h for heat and K_m for momentum transport, respectively. For small eddies, as found in the stable boundary layer, the gradient transport theory (e.g., Stull, 1988) approximates the relationship between the vertical turbulent fluxes and the vertical gradients by

$$H = -\varrho\, c_p\, K_h \cdot \partial_z \bar{\theta} \tag{16}$$

$$\tau = \varrho\, K_m \cdot \sqrt{(\partial_z \bar{u})^2 + (\partial_z \bar{v})^2} \tag{17}$$

(e.g., Wittich and Roth, 1984; Nieuwstadt, 1984b), or

$$K_h = -\frac{\langle w'\theta' \rangle_{P'}}{\partial_z \bar{\theta}} \tag{18}$$

$$K_m = \sqrt{\frac{\langle w'u' \rangle_{P'}^2 + \langle v'u' \rangle_{P'}^2}{(\partial_z \bar{u})^2 + (\partial_z \bar{v})^2}}\,. \tag{19}$$

The turbulent fluxes H and τ were directly calculated from the sub-legs P' using eddy correlation (Equation 6 and 7). To obtain the vertical gradients was more complicated. Since shear and stratification were

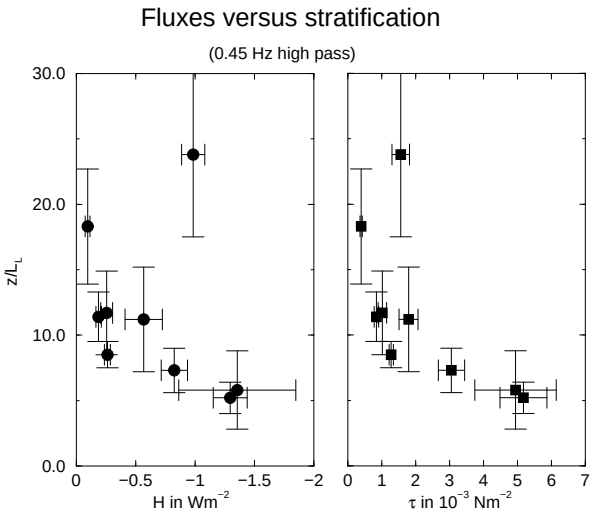

Figure 14. Vertical turbulent fluxes measured in the turbulent regions within the ground-based inversion as function of the dimensionless height z/L_L. The error bars indicate the statistical scatter of the fluxes due to limited measurement distance (Lenschow and Stankov 1986).

changing more or less rapidly on the flight legs due to intermittency, it was necessary to calculate the vertical gradients at the same location and time as each individual turbulent outburst occured, instead of using the gradients obtained from the vertical profiles in Figures 3 and 4. This was achieved by taking advantage of the vertical motion of the HELIPOD during the horizontal flights, which could be interpreted as small vertical soundings along the flight path. After selecting only the turbulent regions of the flight measurements, the turbulence was removed with a low pass filter at $f_C = 1$ Hz ($k_C = 0.157$ m^{-1}), which left the vertical oscillations of the HELIPOD as well as the slower fluctuations of height z untouched. To reduce the sizes of the data sets, the original time series were replaced by series containing the 1 s mean values. Then for each sub-leg a linear approximation $\phi(x, y, z, t)$ (with horizontal coordinates x and y, height z, and time t) was made for the horizontal wind components u and v, and the potential temperature θ for each sub-leg:

$$\phi(x, y, z, t) = m_0 + m_1 x + m_2 y + m_3 z + m_4 t \; . \tag{20}$$

The coefficients m_i, which represented the mean value, the mean spatial gradients, and the time development of quantity $\phi = u, v, \theta$, were calculated using Inverse Modelling (Tarantola, 1987), which in this case was very similar to solving a four dimensional linear equation system using linear regression, but yielded additionally the standard deviations

of the calculated coefficients and their interdependence. This method did not work on all the sub-legs. In some cases Equation 20 was not satisfied with sufficient accuracy because the gradients were changing too fast or the linear approach did not describe the flow. These sub-legs were excluded from the following analysis. On the other hand, on the Southern leg on 18 August the outbursts were comparably short and weak, and the gradients changed very little, so a subdivision into smaller sub-legs was not necessary. Also the northern and the western leg on 19 August were analyzed.

The results of the inverse modelling are added to the time series in Figure 8 (grey lines) to demonstrate the accuracy of this method: On the entire 11 km leg the slow fluctuations of the measured time series of u, v, and θ were approximated very well by the modelled functions (Equation 20), as were the oscillations of the temperature due to the pendulum motion. The oscillations of the wind components u and v were reproduced to the extent that they were caused by the oscillations of height z. The artifact due to inadequate calibration (Section 4) had obviously no affect on the determination of the vertical gradients m_3.

Since the chosen sub-legs and legs were relatively short, no time dependence was observed ($m_4 = 0$). The coefficients m_1 and m_2 were always very small and represented the horizontal gradients on a large scale. The vertical gradients m_3 were calculated with a statistical error of only a few per cent. The variations of height z during the flights, which at first sight only disturbed the measurements, provided an accurate estimation of the vertical gradients of wind and temperature at the same location and time the turbulent outbursts were observed. The vertical gradient of potential temperature ranged between 2.8 and 6.4 K per 100 m, the wind shear in mean wind direction was found between 5.5 and 11 ms^{-1} per 100 m (Table V), with the exception of the western leg on 19 August, where the wind shear was much smaller and therefore nearly no turbulence occured.

Using the locally estimated vertical gradients, the flux Richardson numbers $\mathrm{Ri_f}$ were calculated (Equations 13) for the turbulent regions only and are listed in Table V. While on 19 August the local values of $\mathrm{Ri_f}$ did not differ much from those calculated with the vertical gradients estimated from the vertical profiles in Figures 3 and 4, on 18 August this difference was much larger: $\mathrm{Ri_f}$ was overestimated by a factor of three using the profiles in Figures 3 and 4 and the leg-averaged turbulent fluxes. Using only data obtained in the turbulent regions of the flights yielded flux Richardson numbers between 0.1 and 0.2 on both days, which may be interpreted as typical values for turbulence in this case

rather than the local gradient Richardson number

$$\mathrm{Ri} = \frac{g}{\bar{\theta}} \cdot \frac{\partial_z \bar{\theta}}{(\partial_z \bar{u})^2 + (\partial_z \bar{v})^2} \,, \tag{21}$$

which was found between 0.1 and 0.3 (Table V). The latter is known to be a function of the turbulent Prandtl number Pr in a stable boundary layer, or vice versa. Since the Prandtl number is the quotient of the turbulent diffusivities K_h for heat, and K_m for momentum transport, respectively:

$$\mathrm{Pr} = \frac{K_m}{K_h} \,, \tag{22}$$

the relationship between Pr and Ri gave the opportunity to test whether, if not the turbulent fluxes themselves, at least their ratio and the ratio of the vertical gradients were determined correctly. The results of Pr and Ri are depicted in Figure 15 in a form introduced by Findikakis and Street (1979), together with measured data from other field experiments (Findikakis and Street, 1979; Wittich and Roth, 1984; Yagüe and Cano, 1994) and results from a large eddy simulation (LES) carried out by Schumann and Gerz (1995). With regard to the large scatter of the data found in literature, the measurements with the HELIPOD during DREX agree well with the results found in experiments of the past.

In their summary of measurements and modelling efforts on surface fluxes, Beljaars and Holtslag (1991) stated that the turbulent diffusivities in an intermittent turbulent flow within the surface layer are related to the stratification z/L_* (with Obukhov Length L_*) as

$$K_m \;\propto\; (z/L_*)^{-1} \tag{23}$$

$$K_h \;\propto\; (z/L_*)^{-\frac{3}{2}} \,, \tag{24}$$

and therefore $\mathrm{Pr} \propto \sqrt{z/L_*}$. Figure 14 already intimates that this is also valid for the HELIPOD measurements in the bulk structure of the very stable boundary layer, when L_* is substituted by L_L. In Figure 16 the locally calculated turbulent diffusivities are depicted as a function of the dimensionless height z/L_L. In a double-logarithmic display the data measured in the inversion layer fit rather well the assumptions of Beljaars and Holtslag (1991), made for the surface layer.

7. Summary and conclusions

This case study introduces vertical turbulent fluxes of momentum and heat as measured during the first field campaign (DREX) over land

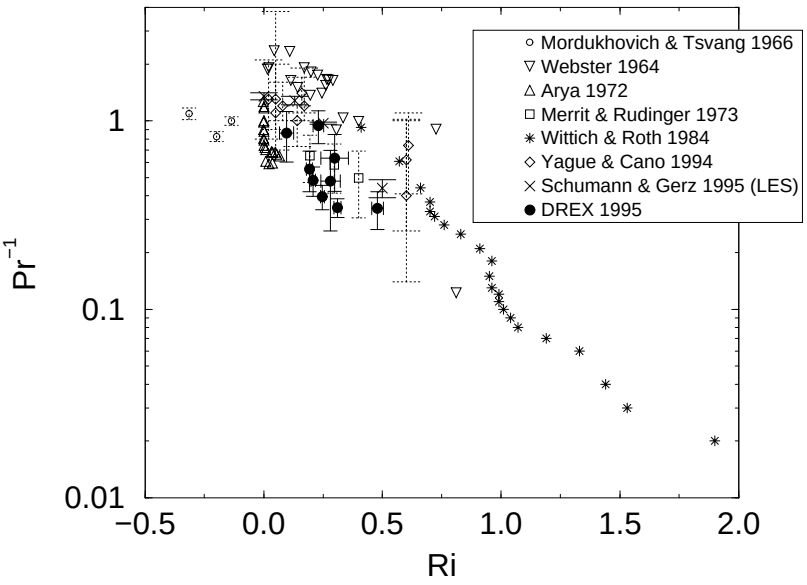

Figure 15. The inverse turbulent Prandtl number Pr as a function of the gradient Richardson number Ri: A comparison of DREX data with other experiments.

with the helicopter-borne, high resolution turbulence measurement system HELIPOD. In the early morning of two days in August, 1995, square flight patterns over flat terrain in North Germany were performed in a neutrally stratified residual layer and a very stably stratified ground-based inversion. In a first analysis, the normal modes of the measurement system and virtual contributions to the fluxes were identified and removed by a high pass filter with a cut off wavelength of 90 m, leaving the turbulent part of the spectra untouched.

In the residual layer the measured vertical fluxes vanished in agreement with the theory, so the system detected the fluxes without significant offset from zero.

Under very stable conditions the vertical motion was largely suppressed due to strong thermal stratification. The onset of vertical turbulent transport was observed in the co-spectra at 60 m wavelength or less, reaching a broad maximum at wavelengths between 12 and 6 m. The turbulence was patchy and intermittent, and the turbulent kinetic energy and the turbulent transport were concentrated in short outbursts. The vertical turbulent fluxes, averaged over straight flight legs of 10 km length, were found at about -0.2 Wm^{-2} (sensible heat) and $1.0 \cdot 10^{-3}$ Nm^{-2} (total horizontal momentum). The statistical errors of the leg-

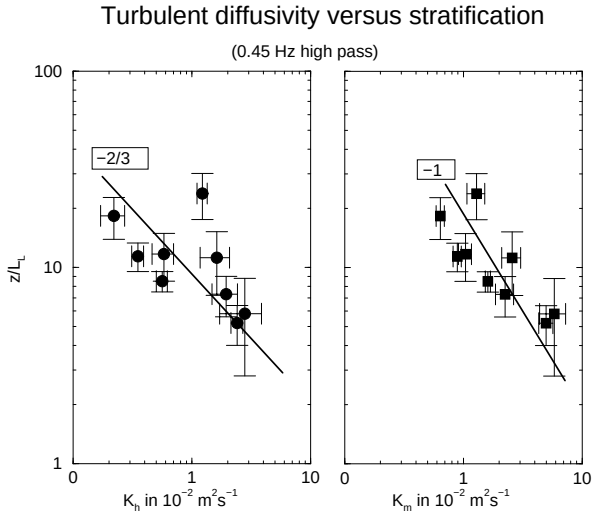

Figure 16. Turbulent diffusivities K_h and K_m versus the dimensionless height z/L_L, as measured in the turbulent regions within the ground-based inversion. For comparison, two lines representing the assumptions of Beljaars and Holtslag (1991) are added.

averaged fluxes, calculated for each leg with the standard method that uses the integral length scale and the flight distance (Lenschow and Stankov, 1986), were very small. A closer view of the intermittent structure of the flow illustrated that the fluxes within the turbulent patches were about five times larger than the averaged values, which is in agreement with the observation that the turbulent outbursts covered about one fifth of the flight, while the rest was nearly non-turbulent. This leads to the presumption, that the method of Lenschow and Stankov (1986), when applied to a very stable and therefore strongly intermittent flow (e.g., Dias et al., 1995), underestimates the statistical scatter of the turbulent fluxes.

The local scales of the very stable flow in the ground-based inversion were calculated using the leg-averaged fluxes. The dimensionless standard deviations of horizontal wind $\sigma_h/u_L \approx 3.3$, vertical wind $\sigma_w/u_L \approx 1.6$, and temperature $\sigma_\theta/\theta_L \approx 5.4$ were in good agreement with the results of other field experiments. Scaling the second-order moments of turbulence with local similarity theory seems to be appropriate even in a very intermittent flow.

The fluxes presented are remarkable for three reasons: 1) they were rather small; 2) their spectral maxima were located at wavelengths that are usually hardly accessible to airborne measurements; and 3) they

were observed by an uncommon and recently developed measurement system. To verify these fluxes by means of comparison with theory and other measurements, the turbulent diffusivities K_m and K_h were estimated for the turbulent outbursts that were responsible for nearly the entire turbulent transport. Since shear and stratification changed rapidly on the flight, the mean vertical gradients were not appropriate to characterize the turbulent flow. The turbulent outbursts had to be isolated from the intermittent flow and treated as individual events. For application of the gradient transport theory, the vertical gradients had to be determined locally. This was achieved by taking advantage of the vertical motions of the measurement system, which could be interpreted as small vertical soundings that accompanied the horizontal flight. The measured series were approximated by a linear approach whose coefficients were calculated with an inverse model.

The turbulent diffusivities K_m and K_h, the Richardson number Ri, and the flux Richardson number $\mathrm{Ri_f}$ of the individual outbursts, were calculated locally by this method. The turbulent outbursts were characterized by $0.1 < \mathrm{Ri_f} < 0.2$ and $0.1 < \mathrm{Ri} < 0.3$. The turbulent Prandtl number Pr ranged between 1.1 and 2.8, which indicates a more efficient exchange of momentum than of heat in the intermittent regime (see Beljaars and Holtslag, 1991; Mahrt, 1998). The relationship between Ri and Pr was found in good agreement with the results of other experiments in the stable boundary layer and a large eddy simulation. Therefore, at least the relationship between the turbulent fluxes and the local gradients within the outbursts observed in this field experiment were determined correctly.

The vertical turbulent transport decreased with increasing thermal stratification, as stated by Mahrt (1998), in the range $5 < z/L_L < 20$. The turbulent diffusivities in the bulk flow were related to the stratification z/L_L as $K_m \propto (z/L_L)^{-1}$ and $K_h \propto (z/L_L)^{-\frac{3}{2}}$, and therefore agreed with the assumptions of Beljaars and Holtslag (1991), made for an intermittent flow in the surface layer.

Although the introduced vertical fluxes could not be verified directly, since there were no comparable measurements available, and existing formulations of the very stable boundary layer are not sufficient, the agreement of the deduced relations with theory and other observations is remarkable. We hope that the case study presented will yield a small contribution to the understanding of the very stably stratified flow above the surface layer.

Acknowledgements

We like to thank C. Wode and M. Schürmann for their help with operating the HELIPOD system. The radio-soundings were performed by U. Busch, M. Schröter, and H. Siebert. The financial funding for the construction of the HELIPOD was provided by the *Bundesministerium für Bildung, Wissenschaft, Forschung und Technologie* (BMBF), contract No. 07 KFT 74. This research was also supported by the BMBF within the project *Wasserkreislauf*, Grant No. 07 VWK 01/6, and by the *Deutsche Forschungsgemeinschaft* (German Science Foundation) through the *Sonderforschungbereich 420 Flugmesstechnik* (Special Research Program 'Flight Measurement Technique').

References

André, J. C. and L. Mahrt: 1982, 'The Nocturnal Surface Inversion and Influence of Clear-Air Radiative Cooling'. *J. Atmos. Sci.* **39**, 864–878.

Andrén, A.: 1995, 'The Structure of Stably Stratified Atmospheric Boundary Layers: A Large-Eddy Simulation Study'. *Quart. J. Roy. Meteorol. Soc.* **121**, 961–985.

Arya, S. P. S.: 1972, 'The Condition for the Maintenance of Turbulence in Stratified Flows'. *Quart. J. Roy. Meteorol. Soc.* **98**, 264–273.

Beljaars, A. C. M. and A. A. M. Holtslag: 1991, 'Flux Parameterization over Land Surfaces for Atmospheric Models'. *J. Appl. Meteorol.* **30**, 327–341.

Büchler, R.: 1993, 'Untersuchungen zum aerodynamischen Störfeld an einer Hubschrauberschleppsonde'. Master's thesis, Institute for Flight Mechanics, Technical University of Braunschweig, Germany, 99 pp. + Appendix.

Caughey, S. J., J. C. Wyngaard, and J. C. Kaimal: 1979, 'Turbulence in the Envolving Stable Boundary Layer'. *J. Atmos. Sci.* **36**, 1041–1052.

Dias, N., W. Brutsaert, and M. L. Wesely: 1995, 'Z-Less Stratification under Stable Conditions'. *Boundary-Layer Meteorol.* **75**, 175–187.

Findikakis, A. and R. Street: 1979, 'An Algebraic Model for Subgrid Scale Turbulence in Stratified Flows'. *J. Atmos. Sci.* **36**, 1934–1949.

Garratt, J.: 1992, *The atmospheric boundary layer.* Cambridge: University Press, 316 pp.

Garratt, J., G. Hess, W. Physick, and P. Bougeault: 1996, 'The Atmosperic Boundary Layer - Advances in Knowledge and Application'. *Boundary-Layer Meteorol.* **78**, 9–37.

Grossman, R. L.: 1984, 'Bivariate Conditional Sampling of Moisture Flux over a Tropical Ocean'. *J. Atmos. Sci.* **41**, 3238–3252.

Grossman, R. L.: 1992, 'Sampling Errors in the Vertical Fluxes of Potential Temperature and Moisture Measured by Aircraft During FIFE'. *J. Geophys. Res.* **97**, 18439 – 18443.

Holtslag, A. A. M. and F. T. M. Nieuwstadt: 1986, 'Scaling the Atmospheric Boundary Layer'. *Boundary-Layer Meteorol.* **36**, 201–209.

Jacobi, C. and R. Roth: 1995, 'Organisierte mesoskalige Störungen in der stabilen planetaren Grenzschicht'. *Meteor. Z., N. F.* **4**, 150–161.

Lenschow, D. H., X. S. Li, C. J. Zhu, and B. B. Stankov: 1988, 'The Stably Stratified Boundary Layer over the Great Plains; Part I: Mean and Turbulent Structure'. *Boundary-Layer Meteorol.* **42**, 95–121.

Lenschow, D. H. and B. B. Stankov: 1986, 'Length Scales in the Convective Boundary Layer'. *J. Atmos. Sci.* **43**, 1198–1209.

Lumley, L. and H. Panofsky: 1964, *The structure of atmospheric turbulence.* New York: John Wiley & Sons, 239 pp.

Mahrt, L.: 1985, 'Vertical Structure and Turbulence in the Very Stable Boundary Layer'. *J. Atmos. Sci.* **42**, 2333–2349.

Mahrt, L.: 1989, 'Intermittency of Atmospheric Turbulence'. *J. Atmos. Sci.* **46**, 79–95.

Mahrt, L.: 1998, 'Stratified Atmospheric Boundary Layers and Breakdown of Models'. *Theoret. Comput. Fluid Dynamics* **11**, 63–279.

Merrit, G. and G. Rudinger: 1973, 'Thermal and Momentum Diffusivity Measurements in a Turbulent Stratified Flow'. *AIAA J.* **11**, 1465–1470.

Mordukhovich, M. I. and L. R. Tsvang: 1966, 'Direct Measurement of Turbulent Flows at Two Heights in the Atmospheric Ground Layer'. *Izv. Atmos. Oceanic Phys.* **2**, 477–486.

Muschinski, A. and C. Wode: 1998, 'First In-Situ Evidence for Co-Existing Sub-Meter Temperature and Humidity Sheets in the Lower Free Troposphere'. *J. Atmos. Sci.* **55**, 2893–2906.

Nieuwstadt, F.: 1984a, 'Some Aspects of the Turbulent Stable Boundary Layer'. *Boundary-Layer Meteorol.* **30**, 31–55.

Nieuwstadt, F.: 1984b, 'The Turbulent Structure of the Stable, Nocturnal Boundary Layer'. *J. Atmos. Sci.* **41**, 2202–2216.

Rogers, D. P., D. W. Johnson, and C. A. Friehe: 1995, 'The Stable Internal Boundary Layer over a Coastal Sea. Part I: Airborne measurements of the mean and turbulence structure'. *J. Atmos. Sci.* **52**, 667–683.

Schlittgen, R. and H. J. Streitberg: 1994, *Zeitreihenanalyse.* München: R. Oldenbourg Verlag, 502 pp.

Schumann, U. and T. Gerz: 1995, 'Turbulent Mixing in Stably Stratified Shear Flows'. *J. Appl. Meteorol.* **34**, 33–48.

Schürmann, M. and C. Wode: 1996, 'HELIPOD - A Turbulence Measurement System for Meteorological Research'. In: *Proc. Second Intl. Airborne Remote Sensing Conference and Exhibition*, Vol. II. San Francisco, CA, 451–452.

Smedman, A.-S.: 1988, 'Observations of a Multi-Level Turbulence Structure in a Very Stable Atmospheric Boundary Layer'. *Boundary-Layer Meteorol.* **44**, 231–253.

Smedman, A.-S.: 1991, 'Some Turbulence Characteristics in Stable Atmospheric Boundary Layer Flow'. *J. Atmos. Sci.* **48**, 856–868.

Sorbjan, Z.: 1986, 'Local Similarity of Spectral and Cospectral Characteristics in the Stable-Continuous Boundary Layer'. *Boundary-Layer Meteorol.,* **35**, 257–275.

Sorbjan, Z.: 1987, 'An Examination of Local Similarity Theory in the Stably Stratified Boundary Layer'. *Boundary-Layer Meteorol.,* **38**, 63–71.

Sorbjan, Z.: 1988, 'Structure of the Stably-Stratified Boundary Layer during the SESAME-1979 Experiment'. *Boundary-Layer Meteorol.,* **44**, 255–266.

Stull, R.: 1988, *Boundary Layer Meteorology.* Dordrecht: Kluver Acad, 666 pp.

Tarantola, A.: 1987, *Inverse Problem Theory.* Amsterdam: Elsevier, 613 pp.

Webster, C. A. G.: 1964, 'An Experimental Study of Turbulence in a Density Stratified Shear Flow'. *J. Fluid Mech.* **19**, 221–245.

Wittich, K.-P.: 1991, 'The Nocturnal Boundary Layer over Northern Germany: An Observational Study'. *Boundary-Layer Meteorol.* **55**, 47–66.

Wittich, K.-P. and R. Roth: 1984, 'A Case Study of Nocturnal Wind and Temperature Profiles over the Inhomogeneous Terrain of Northern Germany with some Considerations of Turbulent Fluxes'. *Boundary-Layer Meteorol.* **28**, 169–186.

Wode, C. and R. Roth: 1996, 'HELIPOD - ein hubschraubergestütztes meteorologisches Meßsystem'. BMFT-Abschlußbericht 07 KFT 74, Institut für Meteorologie und Klimatologie der Universität Hannover. 145 pp.

Wode, C., R. Roth, and M. Schürmann: 1996, 'The Helicopter-Borne Sensor Package HELIPOD - Features and Capabilities of a New Turbulenc Measurement System for Meteorological Research.'. In: *Proc. Second Intl. Airborne Remote Sensing Conference and Exhibition*, Vol. II. San Francisco, CA, 483–491.

Yagüe, C. and J. Cano: 1994, 'The Influence of Stratification on Heat and Momentum Turbulent Transfer in Antarctica'. *Boundary-Layer Meteorol.* **69**, 123–136.